

A discontinuity-capturing neural network with categorical embedding and its application to anisotropic elliptic interface problems

Wei-Fan Hu¹, Te-Sheng Lin², and Ming-Chih Lai²

¹Department of Mathematics, National Central University, Taoyuan 32001, Taiwan

²Department of Applied Mathematics, National Yang Ming Chiao Tung University, Hsinchu 30010, Taiwan

March 20, 2025

Abstract

In this paper, we propose a discontinuity-capturing shallow neural network with categorical embedding to represent piecewise smooth functions. The network comprises three hidden layers, a discontinuity-capturing layer, a categorical embedding layer, and a fully-connected layer. Under such a design, we show that a piecewise smooth function, even with a large number of pieces, can be approximated by a single neural network with high prediction accuracy. We then leverage the proposed network model to solve anisotropic elliptic interface problems. The network is trained by minimizing the mean squared error loss of the system. Our results show that, despite its simple and shallow structure, the proposed neural network model exhibits comparable efficiency and accuracy to traditional grid-based numerical methods.

1 Introduction

A function, which assigns a unique mapping from one set to another, is the most fundamental building block of science and technology. For example, a scalar function can describe the position of a particle along a line over time, and a vector function can represent the velocity field of a flow. More sophisticated examples might be recognizing license plates from video, translating languages from one to another, detecting fraud in transactions, etc. All of these can also be described in terms of functions, but require more powerful representations than just polynomials or trigonometric functions. In fact, due to their strong expressive power, there is nowadays growing interest in using artificial neural networks together with machine learning techniques to handle various applications that are inherently

complex mappings, such as natural language processing [1], self-driving cars [2], financial fraud detection [3], computer vision [4], and disease diagnosis [5], to name a few.

There is also a growing body of literature in the scientific computing community that recognizes the importance of neural networks which have been used for problems that are difficult to solve by traditional methods, such as inverse problems [6], triangulated mesh prediction [7], or solutions exhibiting corner singularities [8]. In terms of its mathematical foundation, the expressivity of neural networks was mathematically justified [9, 10, 11], revealing the fact that continuous functions can be represented by neural network to any precision. With these in mind, one has at hand a powerful function representation ready to solve science problems. Examples include the well-known Physics-Informed Neural Networks (PINNs) [12, 13] and deep Ritz method (DRM) [8], which have led to a proliferation of studies on solving partial differential equations (PDEs) in complex geometries or in high dimensions. From a higher-level perspective, Deep Operator Networks (DeepONet) [14] and Fourier Neural Operator (FNO) [15] directly learn nonlinear operators, mappings from one function to another, which have also received considerable attention.

Nevertheless, when reflecting on the fundamental issue of representing scalar functions using neural networks, we found that there is very limited attention to functions that are not necessarily continuous, despite their common occurrence in practical applications such as composite materials, fluid mechanics, nuclear waste disposal, and various other fields. The expressive power of neural networks for continuous functions was shown by Cybenko [9], while for discontinuous functions, Llanas et al. [16] proved that neural networks can approximate piecewise continuous functions almost uniformly. However, their approach involved using neural networks with continuous activation functions to approximate step functions, resulting in an inevitable overall smoothness of the network function. One may also use discontinuous activation functions in neural networks [17, 18, 19], which is common in electronic circuits with switches and dry friction. These functions have been demonstrated to be effective in linear and quadratic programming tasks [20]. But still, how to train such network functions remains an open research question.

This work aims to introduce a simple methodology to represent a discontinuous function comprising multiple smooth pieces. Several attempts have been made to deal with functions that have two or three pieces, the most intuitive of which is to partition the input space into contiguous regions determined by the points of discontinuity, and then create separate and independent neural network models for each region [21]. However, the number of networks in this approach obviously grows in proportion to the number of domain partitions. One can also rewrite the problem in terms of the weak form loss [22], but the accuracy is limited by the underlying Monte Carlo integrator. Recently, the authors of this paper proposed the Discontinuity-Capturing Shallow Neural Network (DCSNN) [23], a single network architecture that can present piecewise continuous functions. Here we broaden the discussion to functions that comprise multiple (e.g., hundreds or thousands) smooth pieces. The method we employ can be readily applied to address problems involving piecewise continuous solutions.

As a potential application to the proposed neural network model, we consider an anisotropic elliptic interface problem that often appears in the study of incompressible flows with interfaces [24], composite materials, crystal growths, and Hele-Shaw flows. Such a problem plays an important role in many natural phenomena and industrial applications, and is of major interest to the applied mathematics community. The main difficulty in solving the problem is that the anisotropic diffusion tensor is often piecewise continuous and the solution itself is also discontinuous. To tackle the problem numerically, there are nonlinear schemes of the finite volume method for preserving the positivity of the solutions [25, 26], and other approaches [27, 28, 29]. Recently, Li et al. solve the problems with deep neural networks using the first-order formulation [30]. One should note that the solutions in their works are smooth, whereas the problems with interfaces are more challenging since the solutions are only piecewise continuous. Due to the low global regularity of the solution, designing efficient methods is essential and highly nontrivial.

The rest of this article is organized as follows. In Section 2, we illustrate the network structure of DCSNN with multi-piece embedding structure. In Section 3, we explore the application in solving anisotropic elliptic interface problems, and provide concluding remarks in Section 4.

2 Functions with multiple smooth pieces represented by single neural network architecture

We consider a simply connected bounded region $\Omega \subset \mathbb{R}^d$ containing L disjoint subdomains,

$$\Omega_1, \Omega_2, \dots, \Omega_L \subset \Omega, \quad \Omega_i \cap \Omega_j = \emptyset, \quad \text{for } i \neq j.$$

We further define the boundary of each subdomain as Γ_ℓ , and assume that Γ_ℓ form mutually disjoint closed surfaces. The complementary part of all subdomains is represented by Ω_0 so that $\Omega = \bigcup_{\ell=0}^L \Omega_\ell$ (meaning that Ω consists of $L + 1$ disjoint subdomains). See Fig. 1 for an illustrative two-dimensional example with $L = 4$. We now consider a d -dimensional piecewise continuous scalar function $u(\mathbf{x})$ defined in Ω , which is smooth within each subdomain Ω_ℓ and exhibits jump discontinuities across each interface Γ_ℓ .

As discussed earlier, a standard neural network model with a smooth activation function yields representations that are inherently continuous, making them insufficient for capturing jump discontinuities. To effectively approximate such piecewise continuous functions using neural networks, we first revisit our previous work, DCSNN [23], which demonstrates the ability to model discontinuous behavior using a simple shallow neural network architecture. Building upon this foundation, we introduce several classification models that extend and generalize DCSNN.

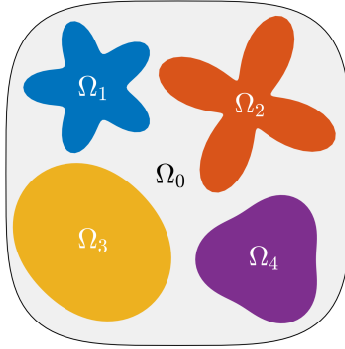


Figure 1: A domain $\Omega = \cup_{\ell=0}^4 \Omega_\ell$ containing four disjoint subdomains.

2.1 Discontinuity capturing shallow neural networks with scalar encoding

We begin by revisiting the core idea of DCSNN [23] and highlighting its capability to approximate piecewise smooth functions. The key observation is that a piecewise continuous function can be mapped to a continuous function in higher-dimensional spaces. This mapping acts like a classification, assigning disjoint subdomains to disconnected sets. For this purpose, we define a categorical scalar function $z : \mathbb{R}^d \rightarrow \mathbb{R}$ as follows:

$$z(\mathbf{x}) = \gamma_\ell \quad \text{if } \mathbf{x} \in \Omega_\ell, \quad (1)$$

where γ_ℓ are predefined constants. A natural choice for γ_ℓ is to assign it as the region index,

$$\gamma_\ell = \ell,$$

with the label representing the subdomain to which the input variable \mathbf{x} belongs. Alternatively, similar to target embedding categorization [31], we can incorporate input data information into the label, and define γ_ℓ based on function averages over each region:

$$\gamma_\ell = \bar{\gamma}_\ell = \frac{\int_{\Omega_\ell} u(\mathbf{x}) \, d\mathbf{x}}{|\Omega_\ell|}.$$

However, these values may not be known if u itself is a function to be found (for instance, when u is the solution of a PDE, see Section 3 for illustration).

We should point out that the choice of the scalar γ_ℓ implicitly introduces an ordering, which significantly impacts subsequent neural network training, especially when dealing with a large number of disjoint subdomains. Determining the optimal constants a priori is generally impractical. Nevertheless, as long as γ_ℓ is different between disjoint regions, the function $\mathbf{x} \rightarrow z(\mathbf{x})$ maps disjoint subdomains to disconnected sets.

Using the scalar categorical encoding function $z(\mathbf{x}) \in \mathbb{R}$, we aim to construct a continuous function extension by augmenting the input variable \mathbf{x} with z . Specifically, we seek an augmented function $U : \mathbb{R}^{d+1} \rightarrow \mathbb{R}$ that satisfies

$$U(\mathbf{x}, z(\mathbf{x})) = u(\mathbf{x}), \quad \text{if } \mathbf{x} \in \Omega. \quad (2)$$

It is worth noting that U is only defined and continuous on a disconnected subset of \mathbb{R}^{d+1} , precisely $\{(\mathbf{x}, z(\mathbf{x})) \in \mathbb{R}^{d+1} \mid \mathbf{x} \in \Omega\}$. However, this function U can be continuously extended to the entire \mathbb{R}^{d+1} space as ensured by the Tietze extension theorem [32]. Consequently, Eq. (2) transforms the piecewise continuous function into the continuous function defined in a space of one higher dimension. The remaining task of DCSNN is to construct a shallow neural network to approximate this augmented continuous function $U(\mathbf{x}, z)$.

Leveraging the strong expressiveness of neural networks, we approximate the extension function U using a neural network, denoted by $U_{\mathcal{N}}$. In its simplest form, the fully-connected one-hidden-layer neural network, $U_{\mathcal{N}}$, can be written as

$$U_{\mathcal{N}}(\mathbf{x}, z(\mathbf{x})) = \sum_{j=1}^N c_j \sigma(W_j[\mathbf{x}, z(\mathbf{x})]^\top + b_j), \quad (3)$$

where N is the number of neurons in the hidden layer, $c_j \in \mathbb{R}$, $W_j \in \mathbb{R}^{1 \times (d+1)}$ are the weights, $b_j \in \mathbb{R}$ are the biases, and σ is the activation function. Finally, we deliberately define the neural function $u_{\mathcal{N}}(\mathbf{x})$ through the intermediate map $U_{\mathcal{N}}$ which represents inherently piecewise continuous functions as

$$u_{\mathcal{N}}(\mathbf{x}) = U_{\mathcal{N}}(\mathbf{x}, z(\mathbf{x})). \quad (4)$$

With the same input, this succinct notation makes it easy to estimate the error between the target function $u(\mathbf{x})$ and the neural network function $u_{\mathcal{N}}(\mathbf{x})$.

In summary, the DCSNN with scalar encoding model can be described as follows. The function $u_{\mathcal{N}}$ consists of two layers, namely, a discontinuity-capturing (DC) layer and a fully-connected (FC) layer. The DC layer maps the input variable \mathbf{x} to $(\mathbf{x}, z(\mathbf{x}))$, which is pre-defined and does not require training. On the contrary, the FC layer consists of N neurons with weights and biases that need to be learned. A schematic illustration of the network structure is shown in Fig. 2. As a result, the DCSNN with scalar encoding comprises a total of $N_p = (d+3)N$ parameters, which need to be found through network training.

2.2 One-hot encoding neural networks

Inspired by one-hot encoding in classification tasks, we propose an alternative representation of the categorical function. Specifically, we define a vector-valued function $\mathbf{z} : \mathbb{R}^d \rightarrow \mathbb{R}^{L+1}$ to represent categorical variables in a binary format:

$$\mathbf{z}(\mathbf{x}) = \delta_{\ell+1}, \quad \text{if } \mathbf{x} \in \Omega_\ell, \quad (5)$$

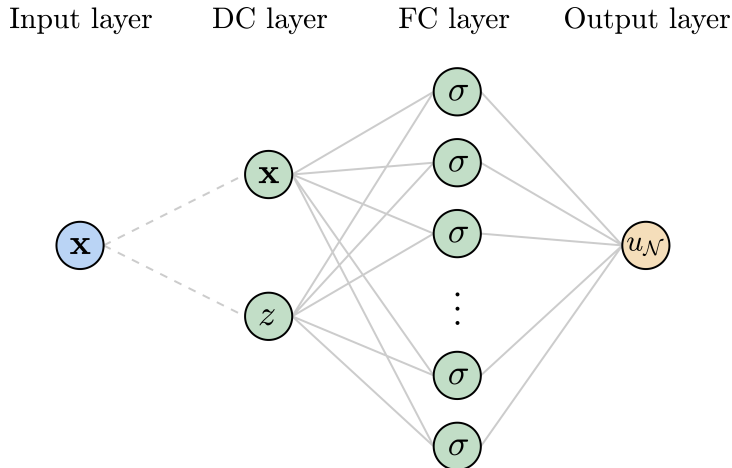


Figure 2: Neural network structure of DCSNN with scalar encoding. The dashed/solid lines denote non-trainable/trainable parameters.

where $\delta_{\ell+1}$ is the standard basis vector in \mathbb{R}^{L+1} (with a 1 at the $(\ell + 1)$ -th position and 0 elsewhere, for $\ell = 0, 1, \dots, L$). This mapping offers the advantage that the distance between the augmented features \mathbf{z} of any two subdomains remains constant, avoiding any implicit ordering in the augmentation coordinate. Mimicking the idea as introduced in the DCSNN with scalar encoding model, we then construct a continuous extension function U that incorporates the vector-valued categorical function \mathbf{z} as follows:

$$U(\mathbf{x}, \mathbf{z}(\mathbf{x})) = u(\mathbf{x}), \quad \text{if } \mathbf{x} \in \Omega. \quad (6)$$

Observe that, in this case the input dimension of U becomes $d + L + 1$. This intermediate map U can again be simply approximated by a shallow network $u_{\mathcal{N}}$ of the form

$$u_{\mathcal{N}}(\mathbf{x}) = U_{\mathcal{N}}(\mathbf{x}, \mathbf{z}(\mathbf{x})) = \sum_{j=1}^N c_j \sigma(W_j[\mathbf{x}, \mathbf{z}]^{\top} + b_j). \quad (7)$$

Notably, the usage of the vector-valued functions as augmented inputs has also been explored in [33], where it was employed to classify two subdomains within their network architecture.

Compared to the scalar encoding model (1), adopting the one-hot encoding model seems ideal in the absence of ordinal or nominal labels for each subdomain. However, approximating this continuous function U using a neural network expression with the augmented input $(\mathbf{x}, \mathbf{z}) \in \mathbb{R}^{d+L+1}$ poses computational challenges as the number of subdomains increases (i.e., larger L). This can lead to a significant increase in the number of learnable parameters that need to be trained. While the unknown parameters of the network expression (7) now become $N_p = (d + L + 3)N$, making the training process computationally intensive.

2.3 Categorical embedding neural networks

From the previous two models, it becomes clear that there are multiple choices for selecting the categorical function. The goal of this function is to create a mapping that elevates each smooth part of the function into higher dimensions while simultaneously separating them. It is therefore evident that there are infinitely many choices for such a function.

In this context, we propose a categorical embedding neural network, where the objective is to *learn* an optimal categorical function. This function aims to effectively capture the intrinsic properties (or features) within the function profiles of each subdomain (or category), and thus map similar categories closer together in a specific low-dimensional space. To this end, we define the categorical function $\mathbf{z} : \mathbb{R}^d \rightarrow \mathbb{R}^D$ via a linear map:

$$\mathbf{z}(\mathbf{x}) = E\boldsymbol{\delta}(\mathbf{x}), \quad (8)$$

where $\boldsymbol{\delta}(\mathbf{x}) = \boldsymbol{\delta}_{\ell+1} \in \mathbb{R}^{L+1}$ for $\mathbf{x} \in \Omega_\ell$, and $E \in \mathbb{R}^{D \times (L+1)}$ is the embedding matrix that classifies the $(L+1)$ subdomains into a low-dimensional embedded space of selected dimension D (with $D \leq L+1$). We remark that the categorical embedding function (8) used here follows the same principle as the entity embedding model [34], where high-cardinality categorical variables are embedded into low-dimensional Euclidean spaces.

Once again, we look for an extension function $U : \mathbb{R}^{d+D} \rightarrow \mathbb{R}$ with the proposed categorical embedding map (8) that satisfies

$$U(\mathbf{x}, \mathbf{z}(\mathbf{x})) = U(\mathbf{x}, E\boldsymbol{\delta}(\mathbf{x})) = u(\mathbf{x}), \quad \text{if } \mathbf{x} \in \Omega. \quad (9)$$

At this stage, the embedding matrix E is treated as an unknown weight and can be learned through standard machine learning optimization techniques. Additionally, we must emphasize that the importance of this categorical step lies in mapping of low-dimensional discontinuous functions into high-dimensional smooth functions.

The next step involves approximating the extension function U by constructing a categorical embedding neural network $u_{\mathcal{N}}$ (through the intermediate map $U_{\mathcal{N}}$) that represents inherently piecewise functions, in the following form:

$$u_{\mathcal{N}}(\mathbf{x}) = U_{\mathcal{N}}(\mathbf{x}, E\boldsymbol{\delta}(\mathbf{x})) = \sum_{j=1}^N c_j \sigma(W_j[\mathbf{x}, E\boldsymbol{\delta}(\mathbf{x})]^\top + b_j), \quad (10)$$

where $c_j \in \mathbb{R}$, $W_j \in \mathbb{R}^{1 \times (d+D)}$ are the weights, and $b_j \in \mathbb{R}$ are the biases. The total parameters to be learned, including weights, biases and embedding matrix E , are $N_p = (d+D+2)N + (L+1)D$.

The categorical embedding DCSNN consists of three layers: a DC layer, a categorical embedding (CE) layer, and a FC layer. The DC layer maps the input variable \mathbf{x} to $(\mathbf{x}, \boldsymbol{\delta}(\mathbf{x}))$, which is predefined and does not require training. In contrast, the CE layer learns the embedding (or weight) matrix E via the mapping $\mathbf{z}(\mathbf{x}) = E\boldsymbol{\delta}(\mathbf{x})$. The FC layer

consists of N neurons with learnable weights and biases. A schematic representation of the network structure is shown in Fig. 3. Our model can easily be extended by deepening the FC layer with more hidden layers or by adding residual connections, but for this work, we focus on the simpler structure defined in (10).

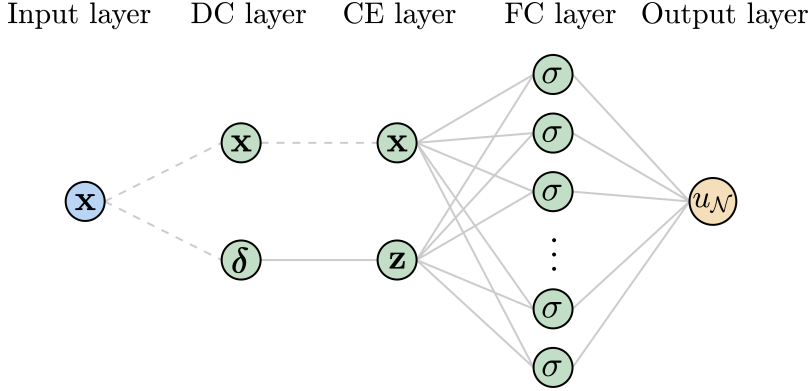


Figure 3: Neural network structure of DCSNN with categorical embedding. The dashed/solid lines denote non-trainable/trainable parameters.

We provide several remarks on the proposed model. Firstly, the categorical embedding technique generalizes both scalar encoding and one-hot encoding models depending on the choice of the embedding matrix E . Particularly, setting $E = [\gamma_0, \gamma_1, \dots, \gamma_L]$ recovers the scalar encoding model (see Eq. (1)), while choosing the identity matrix $E = I_{L+1}$ reverts to the one-hot encoding approach (see Eq. (5)). Secondly, one can also generalize the proposed linear embedding by including nonlinearity. For instance, applying an activation function to the categorical embedding, i.e., setting $\mathbf{z}(\mathbf{x}) = \sigma(E\delta(\mathbf{x}))$, which may enhance the classification of the encoding labels in the embedded space. However, selecting the best low-dimensional embedding, or the optimal reduced dimension D , of the neural network function $u_{\mathcal{N}}$ in Eq. (10) remains a subject of ongoing research. To provide insight into the choice of D , we will present a systematic study of function approximation experiments later in this section. Lastly, the existence of a smooth extension function U on the whole domain again is guaranteed by the Tietze extension theorem [32], ensuring that such a function can be approximated using neural networks for the above three models.

2.4 Discontinuous and derivative properties

We will now discuss the two significant properties of the categorical embedding function $u_{\mathcal{N}}(\mathbf{x})$ in Eq. (10) as follows.

Values at jump discontinuity Generally, the function values of a discontinuous function at a breakpoint hold less significance. Of greater importance is the jump value at the

breakpoint, which represents the difference between the limiting values from two opposite directions. For instance, let us define the boundary of subdomain Ω_1 as Γ_1 , the jump quantity for the function value at $\mathbf{x} \in \Gamma_1$ is given by

$$[u]_{\mathbf{x}} = \lim_{\mathbf{x}^+ \rightarrow \mathbf{x}} u(\mathbf{x}^+) - \lim_{\mathbf{x}^- \rightarrow \mathbf{x}} u(\mathbf{x}^-), \quad (11)$$

where $\mathbf{x}^+ \in \Omega_0$ and $\mathbf{x}^- \in \Omega_1$ (see Fig. 1 for example). It may come as a surprise that this information naturally emerges within the intermediate map U from Eq. (9). That is, taking the categorical function \mathbf{z} in Eq. (8), the limiting value from Ω_0 -side can be evaluated easily by

$$\lim_{\mathbf{x}^+ \rightarrow \mathbf{x}} u(\mathbf{x}^+) = \lim_{\mathbf{x}^+ \rightarrow \mathbf{x}} U(\mathbf{x}^+, \mathbf{z}(\mathbf{x}^+)) = U(\mathbf{x}, E\boldsymbol{\delta}_0), \quad (12)$$

while the other limit is $\lim_{\mathbf{x}^- \rightarrow \mathbf{x}} u(\mathbf{x}^-) = U(\mathbf{x}, E\boldsymbol{\delta}_1)$. Thus the jump value at $\mathbf{x} \in \Gamma_1$, which typically requires taking one-sided limits of the function u , can be calculated directly by evaluating $[u]_{\mathbf{x}} = U(\mathbf{x}, E\boldsymbol{\delta}_1) - U(\mathbf{x}, E\boldsymbol{\delta}_0)$. The same manner applies for the jump of the network function $u_{\mathcal{N}}$ as

$$[u_{\mathcal{N}}]_{\mathbf{x}} = U_{\mathcal{N}}(\mathbf{x}, E\boldsymbol{\delta}_0) - U_{\mathcal{N}}(\mathbf{x}, E\boldsymbol{\delta}_1). \quad (13)$$

The rationale behind this outcome is the smooth nature of the intermediate map U . Consequently, determining the jump quantity can be accomplished easily through function evaluation of the intermediate map, eliminating the need for taking limits of the function.

Derivative evaluation There is also a simple relation between the derivative of the network function $u_{\mathcal{N}}$ and the intermediate map $U_{\mathcal{N}}$. Except at breakpoints, the categorical function $\mathbf{z}(\mathbf{x})$ remains constant everywhere; hence, its derivative is zero, implying that the Jacobian matrix $\nabla \mathbf{z} = \mathbf{0}$. Using chain rule we have

$$\nabla u_{\mathcal{N}} = \nabla_{\mathbf{x}} U_{\mathcal{N}} + \nabla_{\mathbf{z}} \nabla_{\mathbf{z}} U_{\mathcal{N}} = \nabla_{\mathbf{x}} U_{\mathcal{N}}, \quad (14)$$

where ∇ is the usual gradient operator; $\nabla_{\mathbf{x}}$ and $\nabla_{\mathbf{z}}$ denote differentiating only with respect to \mathbf{x} and \mathbf{z} , respectively. As a result, the derivative of $u_{\mathcal{N}}$ can be calculated equivalently by taking the partial derivative of $U_{\mathcal{N}}$ only with the original variables \mathbf{x} . One can also immediately extend the relation for higher-order derivatives.

2.5 Training Method

We train the network function $u_{\mathcal{N}}(\mathbf{x})$ with commonly used mean-squared error loss. As in supervised learning tasks, we approximate the piecewise-defined function $u(\mathbf{x})$ using a neural network. That is, we first choose a set of training data $\{(\mathbf{x}^i, u^i)\}_{i=1}^M$, where

$\mathbf{x}^i \in \Omega$ and $u^i = u(\mathbf{x}^i)$, and specify the embedding function $\mathbf{z}(\mathbf{x})$. The loss function under supervised learning framework is then defined as

$$\text{Loss}(\mathbf{p}) = \frac{1}{M} \sum_{i=1}^M (u^i - u_{\mathcal{N}}(\mathbf{x}^i; \mathbf{p}))^2, \quad (15)$$

where \mathbf{p} is the set of all the trainable parameters.

Throughout this paper, we employ the Levenberg-Marquardt (LM) method [35], which is particularly effective here due to the least-squares loss formulation. The iterative update at the step $k + 1$ in the LM method is expressed as

$$\mathbf{p}^{(k+1)} = \mathbf{p}^{(k)} + (J^\top J + \mu I)^{-1} \left[J^\top (\mathbf{u} - \mathbf{u}_{\mathcal{N}}(\mathbf{p}^{(k)})) \right], \quad (16)$$

where $\mu > 0$ is a tunable damping parameter; \mathbf{u} and $\mathbf{u}_{\mathcal{N}}$ denote the vectors collecting the data u^i and $u_{\mathcal{N}}(\mathbf{x}^i; \mathbf{p})$ in the loss function (15), respectively. Here, J is the Jacobian matrix defined as $\partial \mathbf{u}_{\mathcal{N}}(\mathbf{p}^{(k)}) / \partial \mathbf{p}$. Obviously, the primary computational expense in the LM update step $\Delta \mathbf{p}$ (i.e., the matrix-vector multiplication in the right-hand side of Eq. (16)) arises from solving the regularized least-squares problem with the damping parameter μ . This step is typically performed using Cholesky factorization. However, when $\mu \ll 1$, the condition number of $J^\top J + \mu I$ can become extremely large, leading to instability and poor approximation of the update step. To mitigate this issue, we can compute the parameter update $\Delta \mathbf{p}$ using QR factorization by solving the following linear system:

$$\begin{bmatrix} J \\ \sqrt{\mu} I \end{bmatrix} \Delta \mathbf{p} = \begin{bmatrix} \mathbf{u} - \mathbf{u}_{\mathcal{N}}(\mathbf{p}^{(k)}) \\ \mathbf{0} \end{bmatrix}.$$

Note that the network model with the loss function (15) is conventionally trained using optimizers such as ADAM [36] or L-BFGS [37], which are widely adopted in the literature. In subsequent experiments, we will compare the efficiency of various approaches with these optimizers during the training process.

2.6 Test Examples

We present two examples to illustrate the capability of the proposed CE model, originally introduced as the categorical embedding technique, in approximating piecewise smooth functions. Additionally, we compare its performance with scalar encoding (SE) and one-hot encoding (OH) models. In all network models, we use $N = 50$ neurons in the FC layer, maintaining the same number of basis network functions across different approaches. Each neuron is employed with the sigmoid activation function. For each example, we randomly sample test points approximately 10 times the number of training points to evaluate the average L^2 and L^∞ errors over 10 trial runs. The LM optimizer stops either after 1000 training steps or when the tolerance $\varepsilon = 10^{-15}$ is reached.

Example 1

We consider a domain $\Omega \subset \mathbb{R}^2$ that is enclosed by the superellipse, $x_1^4 + x_2^4 = 1$, which encapsulates four subdomains whose boundaries (or interfaces) are described by the polar curves as $r_1(\theta) = 0.3 - 0.1 \cos(5\theta)$, $r_2(\theta) = 0.35 - 0.2 \sin(4\theta)$, $r_3(\theta) = 0.45 - 0.05 \sin(2\theta)$, $r_4(\theta) = 0.35 - 0.05 \cos(3\theta)$ with the center located at $(-0.5, 0.5)$, $(0.4, 0.4)$, $(-0.5, -0.4)$, $(0.5, -0.5)$, respectively. The domain is depicted Fig. 1. The target function u is chosen as

$$u(x_1, x_2) = \begin{cases} \sin(x_1) \sin(x_2) & \text{if } (x_1, x_2) \in \Omega_0, \\ \exp(x_1 - x_2) & \text{if } (x_1, x_2) \in \Omega_1, \\ \cos(x_1 + x_2) & \text{if } (x_1, x_2) \in \Omega_2, \\ 0.5 \cosh(x_1 + x_2) & \text{if } (x_1, x_2) \in \Omega_3, \\ \ln(x_1 + x_2 + 3) & \text{if } (x_1, x_2) \in \Omega_4. \end{cases} \quad (17)$$

We minimize the loss function (15) using 1000 randomly sampled training points, consisting of 880 points inside the domain Ω and 120 points along the domain boundary $\partial\Omega$.

To demonstrate the training efficiency, we compare the performance of various optimizers discussed in the previous subsection with the three categorical network models. For the scalar encoding model, we particularly set the label values as $\gamma_\ell = \ell$ for $\ell = 0, 1, \dots, 4$.

The results are shown in Fig. 4, where all models exhibit a similar trend. Specifically, the gradient-based ADAM optimizer (purple dash-dotted line) achieves a loss magnitude of approximately 10^{-5} but gets stuck in a local minimum, even after 10000 training steps. Meanwhile, the quasi-Newton L-BFGS algorithm (yellow dotted line) performs slightly better than ADAM but also nearly stagnates, resulting in a slow decrease of the loss value in subsequent steps. In contrast, the LM update strategy using Cholesky decomposition (red dashed line) reaches a local minimum as low as 10^{-15} . As expected, the QR factorization method (blue solid line) achieves even lower loss values, around 10^{-20} , within just a few hundred training steps.

Next, we demonstrate the capability of each network model for approximating the 2D discontinuous function. Using the LM optimizer, the comparison results for all models are summarized in Table 1. For the categorical embedding model, we select the reduced dimension $D = 1$. As anticipated, the one-hot encoding model, which requires the most parameters to be trained, achieves the best prediction accuracy. However, the categorical embedding model, which has approximately half the number of parameters as the one-hot model, yields nearly identical results. Furthermore, although both categorical embedding (with $D = 1$) and scalar encoding models use scalars to categorize each function piece, the categorical embedding model is expected to perform better as it learns the optimal classification map in the embedding space.

Additionally, we present the network profile of the learned categorical embedding function in Fig. 5(a). As shown, the network model accurately captures all jump discontinuities sharply and represents the function well, with the absolute error, depicted in Fig. 5(b), being on the order of 10^{-7} . It is observed that the significant errors mainly occur near the

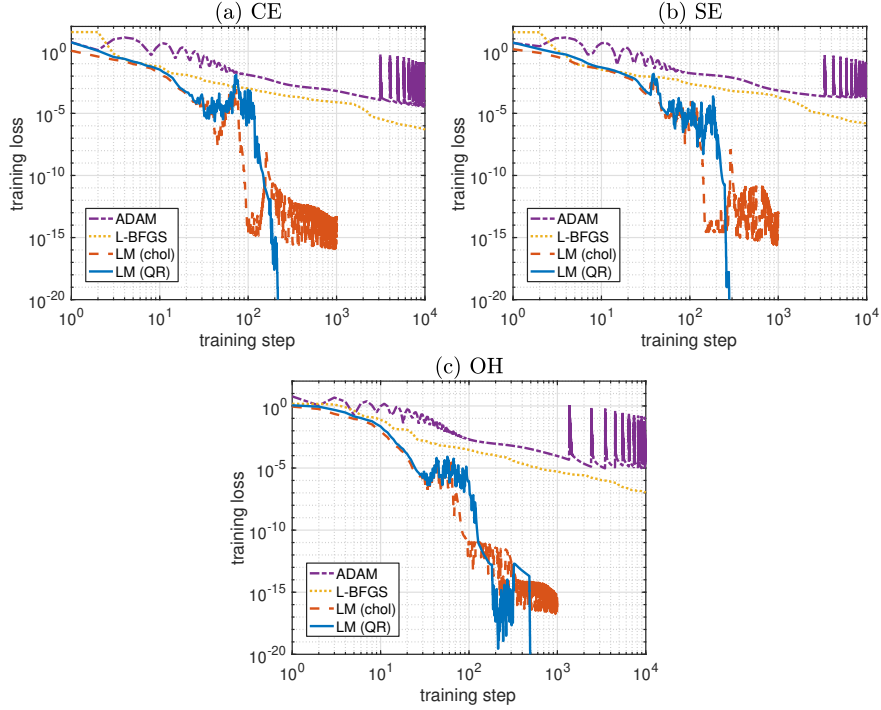


Figure 4: Training history for (a) categorical embedding, (b) scalar encoding, and (c) one-hot encoding model with different optimizers.

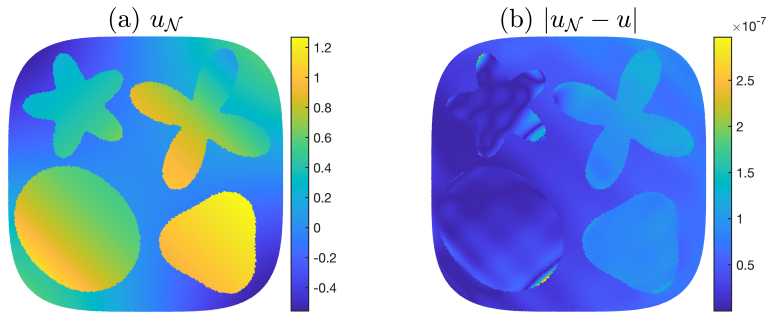


Figure 5: (a) The trained CE model $u_{\mathcal{N}}$ for the piecewise-defined function in Example 1. (b) The absolute error $|u_{\mathcal{N}} - u|$. The maximum error is $\|u_{\mathcal{N}} - u\|_{\infty} = 2.96 \times 10^{-7}$.

interfaces of each subdomain. This is because we only randomly sample the training points within the domain but without additional information along the interfaces.

Table 1: Numerical results of approximating multi-piece function (17). CE: categorical embedding model; SE: scalar encoding model; OH: one-hot encoding model.

Method	N_p	L^2 error	L^∞ error
CE ($D = 1$)	255	6.47E-08	2.09E-06
SE ($\gamma_\ell = \ell$)	250	1.10E-07	4.07E-06
OH	450	4.22E-08	1.06E-06

Example 2

In this example, we demonstrate the expressive power of the proposed CE network by approximating a discontinuous function comprising up to 100 segments. We select a one-dimensional domain $\Omega = [0, 2\pi]$, in which, given random variables a_ℓ , b_ℓ , and c_ℓ , the sub-functions $a_\ell \exp(\sin(b_\ell x) + \cos(c_\ell x))$ are defined within each subdomain $\Omega_\ell = (\Gamma_\ell, \Gamma_{\ell+1})$. Here, the interfaces Γ_ℓ are uniformly distributed with $\Gamma_\ell = \ell \frac{2\pi}{L+1}$. Table 2 summarizes the approximation results for the cases with 5, 10, 50, and 100 subdomains. For the loss model, 1000 training points are sampled in the first three cases, while 2000 points are used for the 100-piece case.

Notably, the one-hot model consistently achieves high prediction accuracy across all cases, succeeding even in the 100-piece case with L^2 error as low as 10^{-8} . However, this model requires the largest number of parameters to learn, resulting in a substantial computational workload. By contrast, regardless of the number of segments, the design of scalar encoding model with given labels (γ_ℓ) requires the same (and least) number of trainable parameters $N_p = 200$. When using a simple nominal label $\gamma_\ell = \ell$, the scalar encoding model performs well for the 5-piece case but fails in other cases. To improve the model’s capability, it is natural to deepen or widen the FC structure in the scalar encoding model. However, our experiments indicate that this strategy still fails to approximate discontinuous functions with many pieces (not shown here). This issue can be easily cured by setting the mean of the target label $\gamma_\ell = \bar{\gamma}_\ell = \int_{\Omega_\ell} u(\mathbf{x}) \, d\mathbf{x} / |\Omega_\ell|$, which can be approximated via Monte Carlo integration. Despite the decrease in prediction accuracy with an increasing number of segments, this labeling strategy consistently enables successful training across all cases, emphasizing the importance of incorporating informative categorical labels.

To investigate the effect of the reduced dimension D in the categorical embedding model, we test various values of D across all cases. For cases with 5 and 10 pieces, setting $D = 1$ is sufficient to achieve highly accurate prediction models with L^2 error as low as 10^{-8} . Increasing D to 2 or 5 provides only a minor improvement in accuracy. However, in the cases with 50 or 100 pieces, a higher-dimensional embedded space may be needed to capture more intrinsic features of the sub-functions. As a result, increasing D generally leads to better approximation outcomes. Our experiments indicate that for cases with a large number of pieces, setting the reduced dimension D to about 10% or 20% of the number of pieces yields a categorical embedding model with comparable accuracy to the

Table 2: Numerical results of approximating one-dimensional multi-piece function with different numbers of pieces in Example 2. CE: categorical embedding model; SE: scalar encoding model; OH: one-hot encoding model. “–” means the method does not converge.

Number of pieces	Method	N_p	L^2 error	L^∞ error
5	CE ($D = 1$)	205	5.65E-08	1.43E-07
	CE ($D = 2$)	260	2.76E-08	8.14E-08
	SE ($\gamma_\ell = \ell$)	200	4.02E-08	3.43E-07
	SE ($\gamma_\ell = \bar{\gamma}_\ell$)	200	9.60E-08	2.19E-07
	OH	400	2.79E-08	7.14E-08
10	CE ($D = 1$)	210	4.27E-08	3.96E-07
	CE ($D = 2$)	270	4.78E-08	1.68E-07
	CE ($D = 5$)	450	3.24E-08	1.87E-07
	SE ($\gamma_\ell = \ell$)	200	–	–
	SE ($\gamma_\ell = \bar{\gamma}_\ell$)	200	3.81E-08	5.67E-07
	OH	650	3.26E-08	1.49E-07
50	CE ($D = 1$)	250	4.03E-04	2.94E-03
	CE ($D = 2$)	350	1.71E-06	2.50E-05
	CE ($D = 5$)	650	3.89E-07	5.29E-06
	CE ($D = 10$)	1150	7.43E-08	1.47E-06
	SE ($\gamma_\ell = \bar{\gamma}_\ell$)	200	8.29E-04	8.92E-03
	OH	2650	4.29E-08	6.00E-07
100	CE ($D = 1$)	300	2.27E-03	1.99E-02
	CE ($D = 2$)	450	1.46E-05	1.92E-04
	CE ($D = 5$)	900	1.94E-07	3.83E-06
	CE ($D = 10$)	1650	9.02E-08	2.83E-06
	SE ($\gamma_\ell = \bar{\gamma}_\ell$)	200	4.47E-03	3.62E-02
	OH	5150	5.69E-08	1.43E-06

one-hot encoding model, while requiring significantly fewer trainable parameters.

3 Anisotropic elliptic interface problems

As a direct application of our proposed model, we consider anisotropic elliptic interface problems, which are challenging to solve by using traditional grid-based numerical methods.

The d -dimensional anisotropic elliptic interface problem with nonhomogeneous jump

conditions is given as follows

$$\nabla \cdot (A(\mathbf{x})\nabla u(\mathbf{x})) - \lambda(\mathbf{x})u(\mathbf{x}) = f(\mathbf{x}) \quad \text{in } \Omega \setminus \bigcup_{\ell=1}^L \Gamma_\ell, \quad (18a)$$

$$[u] = v_\ell(\mathbf{x}), \quad [A\nabla u \cdot \mathbf{n}] = w_\ell(\mathbf{x}) \quad \text{on } \Gamma_\ell, \text{ for } \ell = 1, 2, \dots, L, \quad (18b)$$

where ∇ and $\nabla \cdot$ are the gradient and divergence operators acting on the spatial variable $\mathbf{x} = (x_1, x_2, \dots, x_d)$. Here, $A(\mathbf{x}) \in \mathbb{R}^{d \times d}$ is a positive definite matrix, $\lambda(\mathbf{x})$ is a nonnegative scalar function. Note that both $A(\mathbf{x})$ and $\lambda(\mathbf{x})$ are also piecewise-defined functions which are smooth within each subdomain Ω_ℓ . Recall that the bracket $[\cdot]$ denotes the jump quantity for function values approaching from the Ω_0 side minus the one from the subdomain Ω_ℓ side; \mathbf{n} is the outward normal vector defined on the interface Γ_ℓ (pointing toward the Ω_0 side).

To close the system, a certain boundary condition along $\partial\Omega$ must be given. Throughout this paper, we assume that the solution is imposed by the Dirichlet boundary condition $u(\mathbf{x})|_{\partial\Omega} = g(\mathbf{x})$, while other types of boundary condition (Neumann or Robin type) can be implemented easily without changing the main ingredient of the proposed method (see the implementation in the following).

3.1 Physics-informed neural network (PINN) framework

We employ the categorical embedding model (10) as a solution representation to address the anisotropic elliptic interface problem (18). We now describe the methodology of physics-informed learning machinery [13] for solving Eq. (18) as follows. To find the network parameters in the expression (10), we convert the differential problem to an optimization problem via a loss function. Namely, we first choose the sets of training points in the domain, on the domain boundary, and along all the interfaces, as

$$\{\mathbf{x}^i\}_{i=1}^M \subseteq \Omega, \quad \{\mathbf{x}^j_{\partial\Omega}\}_{j=1}^{M_b} \subseteq \partial\Omega, \quad \{\mathbf{x}^k_{\Gamma_\ell}\}_{k=1}^{M_{\Gamma_\ell}} \subseteq \Gamma_\ell,$$

respectively. The loss function is then defined as

$$\begin{aligned} \text{Loss}(\mathbf{p}) &= \frac{1}{M} \sum_{i=1}^M (\nabla \cdot (A(\mathbf{x}^i)\nabla u_{\mathcal{N}}(\mathbf{x}^i)) - \lambda(\mathbf{x}^i)u_{\mathcal{N}}(\mathbf{x}^i) - f(\mathbf{x}^i))^2 \\ &+ \frac{1}{M_b} \sum_{j=1}^{M_b} (u_{\mathcal{N}}(\mathbf{x}^j_{\partial\Omega}) - g(\mathbf{x}^j_{\partial\Omega}))^2 \\ &+ \sum_{\ell=1}^L \frac{1}{M_{\Gamma_\ell}} \left(\sum_{k=1}^{M_{\Gamma_\ell}} ([u_{\mathcal{N}}] - v_\ell(\mathbf{x}^k_{\Gamma_\ell}))^2 + ([A\nabla u_{\mathcal{N}} \cdot \mathbf{n}] - w_\ell(\mathbf{x}^k_{\Gamma_\ell}))^2 \right), \end{aligned} \quad (19)$$

which consists of the mean squared residual for each equation in the original problem, following the same principle as the PINN-type loss [12, 13]. We also recall that \mathbf{p} represents the set trainable parameters, and the objective is to find a \mathbf{p} that minimizes the loss function. As each term in the loss again takes the form of least-squared errors, we can train the model efficiently using the LM algorithm.

As mentioned in Sec. 2.4, we recall that the categorical function $\mathbf{z}(\mathbf{x})$ is a piecewise constant vector function that has zero derivative over the interior of each subdomain, so that computing derivatives of $u_{\mathcal{N}}$, such as gradient or divergence, can be straightforwardly done using chain rule without any difficulty. For example, recall the relation (14), we have

$$\nabla u_{\mathcal{N}}(\mathbf{x}) = \nabla_{\mathbf{x}} U_{\mathcal{N}}(\mathbf{x}, \mathbf{z}), \quad \mathbf{x} \in \Omega \setminus \bigcup_{\ell=1}^L \Gamma_{\ell}, \quad (20)$$

where $U_{\mathcal{N}}$ is the intermediate map and $\nabla_{\mathbf{x}}$ is the gradient operator with respect to the \mathbf{x} variable only. Therefore, all the derivatives in Eq. (19) are well-defined. As regards the jump conditions in Eq. (19), they can also be computed easily through just function evaluations of $U_{\mathcal{N}}$ (see Subsection 2.4). Similarly, the computation for the flux jump $[A\nabla u_{\mathcal{N}} \cdot \mathbf{n}]$ can be evaluated in the same manner as $[u_{\mathcal{N}}]$.

Moreover, we should point out that the derivative terms involved in the loss model are commonly computed via auto differentiation. But in fact, thanks to the design of the shallow network structure (10), one can easily write down the explicit form of derivatives that is much more efficient in practice. For example, partial derivative with respect to the k -th spatial component is obtained by

$$\frac{\partial u_{\mathcal{N}}}{\partial x_k}(\mathbf{x}) = \frac{\partial U_{\mathcal{N}}}{\partial x_k}(\mathbf{x}, \mathbf{z}) = \sum_{j=1}^N c_j W_{jk} \sigma'(W_j[\mathbf{x}, \mathbf{z}]^{\top} + b_j), \quad (21)$$

where W_{jk} is the k -th component of the vector W_j ; the prime notation of σ means the derivative of the activation function. We mention that both the higher order or mixed partial derivatives to the target function and the Jacobian matrix (collecting all partial derivatives with respect to the learning parameters \mathbf{p} for each residual loss in Eq. (19)) involved in the LM training iteration can be implemented straightforwardly using the simple formulation (10). We also point out that since only simple structure with moderate number of neurons is employed in the present network, the computational complexity and learning workload can be significantly reduced.

3.2 Results

Here we present several examples for solving the anisotropic elliptic interface problems from one- to three-dimensions. To evaluate the performance of the proposed method, for each case we derive the terms $f(\mathbf{x})$, $g(\mathbf{x})$, $v_{\ell}(\mathbf{x})$, and $w_{\ell}(\mathbf{x})$ from the exact solution

$u(\mathbf{x})$, coefficient matrix $A(\mathbf{x})$, and scalar function $\lambda(\mathbf{x})$. With the knowledge of these terms we then train the model to minimize the loss function (19). The training procedure is terminated when the loss value is smaller than a prescribed tolerance $\varepsilon = 10^{-15}$ or reaching 1000 training iterations. In Example 1 to Example 4 we deploy $N = 50$ neurons in the FC layer, while $N = 100$ neurons for Example 5. We also recall that the scalar encoding and one-hot encoding models are applied in the PINN-type loss (19) simply by fixing $E = [\gamma_0, \gamma_1, \dots, \gamma_L]^\top$ and $E = I_{L+1}$, respectively. Again, we report the average L^2 and L^∞ errors using randomly sampled test points, which are 10 times the number of interior training points M , over 10 trial runs for each case.

Example 1

In the first example, we demonstrate the capability of the proposed CE models for solving one-dimensional anisotropic problems with numerous jump discontinuities. Following the same setup as in Example 2 of Subsection 2.6, we uniformly partition the domain $\Omega = [0, 2\pi]$ into subdomains $\Omega_\ell = (\Gamma_\ell, \Gamma_{\ell+1})$ with $\Gamma_\ell = \ell \frac{2\pi}{L+1}$. In each subdomain, the exact solution is given by $u(x) = a_\ell \exp(\sin(b_\ell x) + \cos(c_\ell x))$, the anisotropic coefficient by $A(x) = d_\ell x^2$, and $\lambda(x) = \sin^2(e_\ell x)$, with random variables $(a_\ell, b_\ell, c_\ell, d_\ell, e_\ell)$. Notice that here we choose exactly the same random variables a_ℓ, b_ℓ and c_ℓ as in the function approximation case by fixing the random seed.

The results for cases with 5, 10, 50, and 100 pieces are reported in Table 3, exhibiting trends similar to those observed in the function approximation tests in the previous section. As expected, the one-hot encoded categorization model performs effectively across all cases, achieving accuracy with L^2 errors on the order of 10^{-8} , though this comes with a tradeoff between prediction accuracy and training cost due to the large number of learnable parameters. On the other hand, the scalar encoding with nominal labeling $\gamma_\ell = \ell$ succeeds only in the 5-piece case. As encountered in the function approximation experiments, this can be addressed by assigning a more informative mean value to γ_ℓ . Here, we use the mean of the right-hand side function f by setting $\bar{f}_\ell = \int_{\Omega_\ell} f(x) dx / |\Omega_\ell|$, and normalize those mean values to assign $\gamma_\ell = \bar{\gamma}_\ell = \bar{f}_\ell / \max_{1 \leq \ell \leq L+1} |\bar{f}_\ell|$ in the embedding matrix since the \bar{f}_ℓ values range from 10^{-3} to 10^3 in this experiment. This allows the scalar-encoding model to solve cases with 5 and 10 pieces, but remains insufficient for the cases with more than 50 pieces, leaving an open question regarding selecting appropriate labels γ_ℓ .

Setting the reduced dimension $D = 1$ or 2 in the categorical embedding model performs effectively for the 5- and 10-piece cases, achieving accuracy comparable to the one-hot encoding model. However, unlike in the function approximation context, a low-dimensional embedded space in 50- and 100-piece cases may be inadequate to capture the intrinsic features of the network solution at the PDE level using the PINN learning framework. As observed, increasing the reduced dimension D up to 5 and 10 significantly enhances the model's capability, allowing it to learn the complex network solutions required for the 50- and 100-piece cases.

Table 3: Numerical results of solving the one-dimensional anisotropic elliptic interface problem with different numbers of pieces in Example 1. CE: categorical embedding model; OH: one-hot encoding model. “–” means the method does not converge.

Number of pieces	Method	N_p	L^2 error	L^∞ error
5	CE ($D = 1$)	205	4.37E-07	1.78E-06
	CE ($D = 2$)	260	6.13E-08	1.47E-07
	SE ($\gamma_\ell = \ell$)	200	7.63E-07	4.01E-06
	SE ($\gamma_\ell = \tilde{\gamma}_\ell$)	200	6.40E-07	2.71E-06
	OH	400	2.57E-08	7.69E-08
10	CE ($D = 1$)	210	1.68E-06	4.68E-06
	CE ($D = 2$)	270	2.32E-07	6.43E-07
	SE ($\gamma_\ell = \ell$)	200	–	–
	SE ($\gamma_\ell = \tilde{\gamma}_\ell$)	200	1.36E-03	3.25E-03
	OH	650	7.00E-08	2.20E-07
50	CE ($D = 5$)	650	2.38E-05	1.44E-04
	CE ($D = 10$)	1150	2.26E-05	9.29E-05
	SE ($\gamma_\ell = \tilde{\gamma}_\ell$)	200	–	–
	OH	2650	3.47E-08	8.04E-07
100	CE ($D = 5$)	900	5.77E-05	3.29E-04
	CE ($D = 10$)	1650	4.97E-05	1.94E-04
	SE ($\gamma_\ell = \tilde{\gamma}_\ell$)	200	–	–
	OH	5150	8.08E-08	4.23E-07

Example 2

Next, we turn to solve a two-dimensional problem with anisotropic variable coefficients, which often serves as a benchmark tested in various numerical methods, see [27, 28, 38]. The designated domain is a regular square $\Omega = [-1, 1]^2$ containing a heart-shaped interface $\Gamma_1 = \{(r(\theta) \cos \theta - 0.25, r(\theta) \sin \theta) | r(\theta) = (1 + \cos \theta)/3, \theta \in [0, 2\pi)\}$, which partitions the domain into two subdomains, $\Omega = \Omega_0 \cup \Omega_1$. The exact solution is given by

$$u(x_1, x_2) = \begin{cases} x_1^2 + x_2^2 & \text{if } (x_1, x_2) \in \Omega_0, \\ \exp(x_1) \cos(x_2) & \text{if } (x_1, x_2) \in \Omega_1. \end{cases}$$

Define

$$A_1(x_1, x_2) = \begin{bmatrix} x_1^2 + x_2^2 + 1 & x_1^2 + x_2^2 \\ x_1^2 + x_2^2 & x_1^2 + x_2^2 + 2 \end{bmatrix},$$

and $\lambda_1(x_1, x_2) = \exp(x_1)(x_1^2 + x_2^2 + 3) \sin(x_2)$, the anisotropic coefficient A and the scalar function λ are piecewise spatial dependent functions set by

$$A(x_1, x_2) = \begin{cases} 1000A_1(x_1, x_2) & \text{if } (x_1, x_2) \in \Omega_0, \\ A_1(x_1, x_2) & \text{if } (x_1, x_2) \in \Omega_1, \end{cases}$$

$$\lambda(x_1, x_2) = \begin{cases} 1000\lambda_1(x_1, x_2) & \text{if } (x_1, x_2) \in \Omega_0, \\ \lambda_1(x_1, x_2) & \text{if } (x_1, x_2) \in \Omega_1, \end{cases}$$

so that the contrasts for both functions are 1000.

In this test, we train the loss model using randomly selected training points with $(M, M_b, M_{\Gamma_1}) = (324, 72, 72)$. The results, compared with those from the finite volume method (FVM) [27], are presented in Table 4. Notice that for FVM, the total number of degrees of freedom (or unknowns) is based on the number of discretization grid points, m^2 . As shown in Table 4, FVM uses a grid resolution of $m = 128$, resulting in $N_p = 16384$ unknowns, while the neural network models require only a few hundred parameters. As noted, with a relatively small training dataset (a few hundred points) and a moderate number of trainable parameters (also in the few hundred range), all neural network models achieve higher accuracy than FVM. Given that the solution involves only two subdomain solutions, all models are capable of achieving similar levels of prediction accuracy.

Table 4: Numerical results of solving the two-dimensional anisotropic interface problem in Example 2. CE: categorical embedding model; SE: scalar encoding model; OH: one-hot encoding model; FVM: finite volume method [27].

Method	N_p	L^2 error	L^∞ error
CE ($D = 1$)	252	5.97E-08	5.43E-07
SE ($\gamma_\ell = \ell$)	250	6.62E-08	6.23E-07
OH	300	1.47E-08	1.34E-07
FVM [27]	16384	1.80E-04	

The categorical embedding solution with reduced dimension $D = 1$ is depicted in Fig. 6(a). As shown, the model captures the jump discontinuity sharply along the interface, and the absolute error, depicted in Fig. 6(b), exhibits a pointwise error as low as 10^{-8} , demonstrating the high prediction accuracy of our proposed model. It is worth noting that, in this example, a cusp occurs at $(-0.25, 0)$, our discontinuity capturing models are able to handle such interfaces without any difficulty, whereas some existing numerical methods may encounter challenges with these singular points.

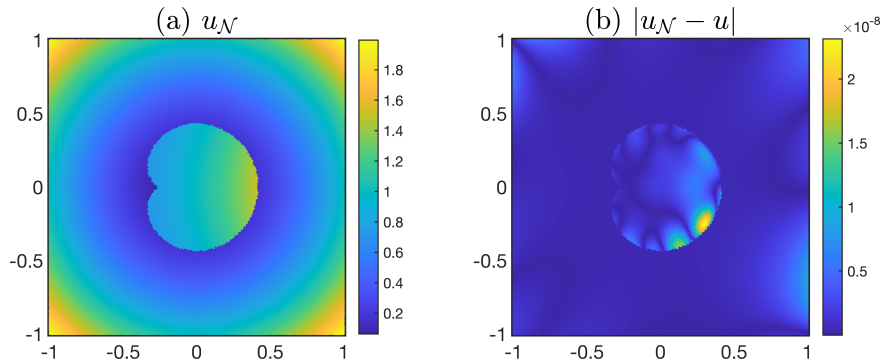


Figure 6: (a) The trained CE model $u_{\mathcal{N}}$ for the piecewise-defined solution of Example 2. (b) The absolute error $|u_{\mathcal{N}} - u|$. The maximum error is $\|u_{\mathcal{N}} - u\|_{\infty} = 2.31 \times 10^{-8}$.

Example 3

In this example we consider a benchmark for 2D variable coefficient elliptic interface problem, see Example 4 in [39]. With a square domain, $\Omega = [-1, 1]^2$, the interface is described as a “chessboard” domain (see the left panel of Fig. 7) given by the zero level set of $\phi(x_1, x_2) = (\sin(5\pi x_1) - x_2)(-\sin(5\pi x_2) - x_1)$. Thus we define the separated domain $\Omega_0 = \{(x_1, x_2) | \phi(x_1, x_2) > 0\}$ and $\Omega_1 = \{(x_1, x_2) | \phi(x_1, x_2) < 0\}$. The diffusion coefficient is given by

$$A(x_1, x_2) = \begin{cases} x_1 x_2 + 2 & \text{if } (x_1, x_2) \in \Omega_0, \\ x_1^2 - x_2^2 + 3 & \text{if } (x_1, x_2) \in \Omega_1. \end{cases}$$

We set $\lambda = 0$ and the exact solution

$$u(x_1, x_2) = \begin{cases} 4 - x_1^2 - x_2^2 & \text{if } (x_1, x_2) \in \Omega_0, \\ x_1^2 + x_2^2 & \text{if } (x_1, x_2) \in \Omega_1. \end{cases}$$

We follow the same setup as in Example 2. The categorical embedding prediction solution with $D = 1$ along with its absolute error is displayed in Fig. 7. The present model is able to achieve a very accurate result with the L^{∞} error $\|u_{\mathcal{N}} - u\|_{\infty} = 5.65 \times 10^{-9}$.

We summarize the accuracy between the present network models and the one of finite element method (FEM) [39] in Table 5. It can be immediately seen that, the prediction accuracy of all models clearly outperforms the one obtained by FEM; the network model with just hundred of trainable parameters readily achieves high solution expressivity with accuracy of order 10^{-9} in L^2 error. It is important to underline that, although this problem can be properly dealt with traditional numerical methods such as FVM or FEM, these methods require identifying regular and irregular grid points (or cell triangulations) as a preliminary step, making their implementation somewhat tedious. On the contrary, it is straightforward to implement the present network models simply using the categorization

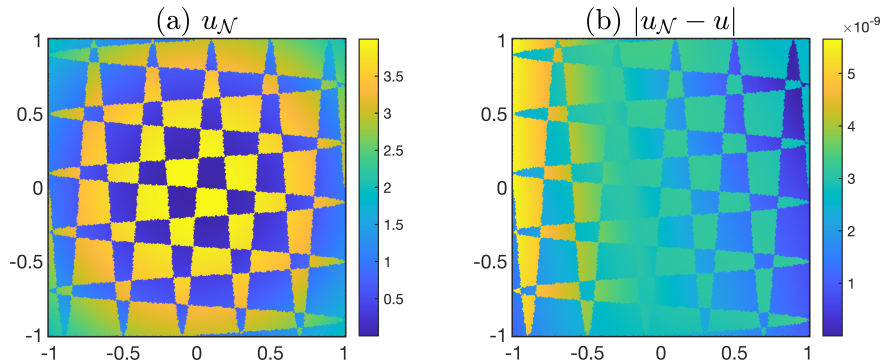


Figure 7: (a) The trained categorical embedding solution $u_{\mathcal{N}}$ with $D = 1$ of Example 3. (b) The absolute error $|u_{\mathcal{N}} - u|$. The maximum error is $\|u_{\mathcal{N}} - u\|_{\infty} = 5.65 \times 10^{-9}$.

map \mathbf{z} . Moreover, we just choose $m_{\Gamma_1} = 72$ randomly sampled points to represent the interface, and the implementation of the optimization algorithm requires no additional effort to those in Example 1 and 2, showcasing the robustness of the present method regardless of the complexity of embedded interface geometries.

Table 5: Numerical results of solving the two-dimensional anisotropic interface problem in Example 3. CE: categorical embedding model; SE: scalar encoding model; OH: one-hot encoding model; FEM: finite element method [39].

Method	N_p	L^2 error	L^∞ error
CE ($D = 1$)	252	4.39E-09	9.59E-09
SE ($\gamma_\ell = \ell$)	250	5.48E-09	1.25E-08
OH	300	4.13E-09	7.89E-09
FEM [39]	102400		2.60E-05

Example 4

In this example we aim to highlight the capability of the present method by tackling two-dimensional problems with multiple subdomains enclosed in an irregular domain. Here, the domain and subdomain geometries are shown in Fig. 1, while the detailed formulation can be found in Example 1 of Subsection 2.6. The solution profile is given in Eq. (17); the coefficient matrix A and scalar function λ in Ω_0 are respectively set by

$$A_0(x_1, x_2) = \begin{bmatrix} (x_1 + x_2)^2 + 1 & -x_1^2 + x_2^2 \\ -x_1^2 + x_2^2 & (x_1 - x_2)^2 + 1 \end{bmatrix} \quad \text{and} \quad \lambda_0(x_1, x_2) = \exp(x_1 - x_2),$$

while in the other subdomains we set $A_\ell(x_1, x_2) = \beta_\ell A_0(x_1, x_2)$ and $\lambda_\ell(x_1, x_2) = \beta_\ell \lambda_0(x_1, x_2)$, where $\beta_1 = 10^{-1}$, $\beta_2 = 10^{-2}$, $\beta_3 = 10^1$, and $\beta_4 = 10^2$ (so the largest ratio in this case is

10000).

Following the same training setup as in Example 2, each solution model achieves high prediction accuracy, with L^2 errors as low as 10^{-9} , as shown in Table 6. Notably, at the PDE-solving level, the categorical embedding model requires only about half the number of learnable parameters compared to the one-hot encoding model. Additionally, owing to the mesh-free nature of the neural network method, implementing the model is straightforward, as demonstrated in this test with the superellipse. In contrast, grid-based methods require substantially greater effort in implementation to solve problems on irregular domains with multiple subdomains.

Table 6: Numerical results of solving the two-dimensional anisotropic interface problem in Example 4. CE: categorical embedding model; SE: scalar encoding model; OH: one-hot encoding model.

Method	N_p	L^2 error	L^∞ error
CE ($D = 1$)	255	2.33E-09	2.28E-08
SE ($\gamma_\ell = \ell$)	250	3.96E-09	3.54E-08
OH	450	2.95E-09	2.09E-08

Example 5

In the last example, we illustrate the robustness of our method for solving a three-dimensional anisotropic problem with multiple interfaces. We set the domain Ω with a super-quadric boundary $x_1^4 + x_2^4 + 16x_3^4 = 1$, in which there are four subdomains, Ω_1 , Ω_2 , Ω_3 , and Ω_4 , encapsulated by four spheres of radius 0.4 with their center respectively located at $(-0.45, 0.45, 0)$, $(0.45, 0.45, 0)$, $(-0.45, -0.45, 0)$, and $(0.45, -0.45, 0)$. See the domain depiction in Fig. 8.

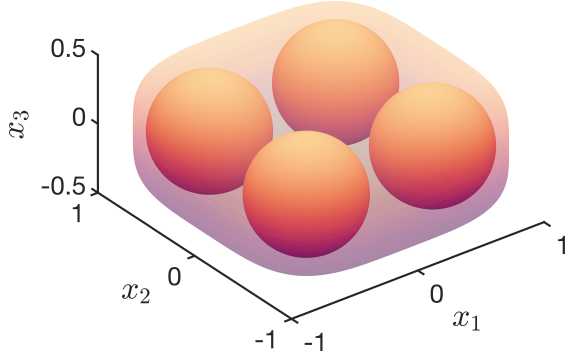


Figure 8: The super-quadric domain $x_1^4 + x_2^4 + 16x_3^4 = 1$ with four embedded spheres of radius 0.4 located at $(-0.45, 0.45, 0)$, $(0.45, 0.45, 0)$, $(-0.45, -0.45, 0)$, and $(0.45, -0.45, 0)$.

Denoting $\mathbf{x} = (x_1, x_2, x_3)$, we set the solution as

$$u(\mathbf{x}) = \begin{cases} \exp(x_1 + x_2 + x_3) & \text{if } \mathbf{x} \in \Omega_0, \\ \sin x_1 \sin x_2 \sin x_3 & \text{if } \mathbf{x} \in \Omega_1, \\ \cos x_1 \cos x_2 \cos x_3 & \text{if } \mathbf{x} \in \Omega_2, \\ \sinh x_1 \sinh x_2 \sinh x_3 & \text{if } \mathbf{x} \in \Omega_3, \\ \cosh x_1 \cosh x_2 \cosh x_3 & \text{if } \mathbf{x} \in \Omega_4, \end{cases} \quad (22)$$

and choose $A_0(\mathbf{x}) = R\Lambda R^T$ and $\lambda_0(\mathbf{x}) = \exp(x_1 - x_2 - x_3)$, where

$$R = \begin{bmatrix} 2/3 & 1/3 & 2/3 \\ -2/3 & 2/3 & 1/3 \\ 1/3 & 2/3 & -2/3 \end{bmatrix} \quad \text{and} \quad \Lambda = \begin{bmatrix} \|\mathbf{x}\|^2 + 1 & 0 & 0 \\ 0 & \|\mathbf{x}\|^2 + 2 & 0 \\ 0 & 0 & \|\mathbf{x}\|^2 + 3 \end{bmatrix}.$$

We further define $A_\ell = \beta_\ell A_0$ and $\lambda_\ell = \beta_\ell \lambda_0$, where $\beta_1 = 0.1$, $\beta_2 = 0.05$, $\beta_3 = 10$, and $\beta_4 = 50$, resulting in a maximum contrast ratio of 1000. In Table 7, we train each model using $(M, M_b, M_\Gamma) = (324, 144, 144)$. In this setup, the categorical embedding network with $D = 1$ and the one-hot encoding model exhibit similar performance, achieving approximately one order of magnitude higher prediction accuracy than the scalar encoding model. Notably, the categorical embedding model learns the categorization map using a single-dimensional representation, leveraging the derivative information provided in the loss model (19). This results in roughly half the number of trainable parameters compared to the one-hot encoding model, significantly reducing computational effort.

Table 7: Numerical results of solving the three-dimensional anisotropic interface problem in Example 5. CE: categorical embedding model; SE: scalar encoding model; OH: one-hot encoding model.

Method	N_p	L^2 error	L^∞ error
CE ($D = 1$)	605	3.42E-08	2.64E-07
SE ($\gamma_\ell = \ell$)	600	2.87E-07	3.45E-06
OH	1000	4.25E-08	5.51E-07

4 Conclusion

In this paper, we propose a single neural network architecture to represent piecewise smooth functions. The proposed network comprises three hidden layers: a discontinuity-capturing layer, a categorical embedding layer, and a fully-connected layer. The discontinuity-capturing layer focuses on mapping domain segments to disconnected sets in a higher-dimensional space, the categorical embedding layer maps high-dimensional information to

a lower-dimensional space, while the fully-connected layer aims to represent the continuous mapping. Under such a design, we show that a piecewise smooth function, even with a large number of pieces, can be approximated by a single neural network with high prediction accuracy. Furthermore, the proposed network function possesses two significant features. First, it enables direct calculation of the jump value at the interfaces. Second, derivatives are well-defined at any point away from the interfaces and domain boundary, making derivative evaluations straightforward.

We then leverage the proposed discontinuity capturing shallow neural network with categorical embedding model to solve traditionally challenging anisotropic elliptic interface problems. The network is trained using the LM optimizer by minimizing the mean squared error loss of the system. With such a simple design and shallow network architecture, the model solves the anisotropic elliptic interface problem with efficiency and accuracy comparable to the existing grid-based numerical methods. We should also point out that the implementation of the present neural network approach is mesh-free. As long as the training points are chosen properly, the loss function and optimization require no further modification for different domain and subdomain geometries.

Finally, we provide evidence that machine learning approaches can achieve accuracy comparable to traditional scientific computing methods and can be of practical use for computational physics applications that often require high fidelity. There are obvious advantages of neural network approaches such as mesh-free, easy to implement, taking full advantages of GPU computation and generalizing easily to high-dimensional problems.

Acknowledgments

W.-F. Hu, T.-S. Lin and M.-C. Lai acknowledge the supports by National Science and Technology Council, Taiwan, under research grant 111-2115-M-008-009-MY3, 111-2628-M-A49-008-MY4 and 110-2115-M-A49-011-MY3, respectively. W.-F. Hu and T.-S. Lin also acknowledge the supports by National Center for Theoretical Sciences, Taiwan.

References

- [1] T. Young, D. Hazarika, S. Poria, E. Cambria, “Recent Trends in Deep Learning Based Natural Language Processing”, *IEEE Comput. Intell. Mag.*, vol. 13, pp. 55–75, 2018.
- [2] S. Grigorescu, B. Trasnea, T. Cocias, G. Macesanu, “A survey of deep learning techniques for autonomous driving”, *J. Field Robot.*, vol. 37, pp. 362–386, 2020.
- [3] A. Roy, J. Sun, R. Mahoney, L. Alonzi, S. Adams, P. Beling, “Deep learning detecting fraud in credit card transactions”, *2018 Systems and Information Engineering Design Symposium (SIEDS)*, pp. 129–134, 2018.

- [4] N. Jin, Y. Zhu, Z. Geng, R. Fedkiw, “A Pixel-Based Framework for Data-Driven Clothing”, arXiv:1812.01677, 2018.
- [5] D. J. Park, M. W. Park, H. Lee, Y. J. Kim, Y. Kim, Y. H. Park, “Development of machine learning model for diagnostic disease prediction based on laboratory tests”, *Sci. Rep.*, vol. 11, pp. 7567, 2021.
- [6] S. Pakravan, P. A. Mistani, M. A. Aragon-Calvo, F. Gibou, “Solving inverse-PDE problems with physics-aware neural networks”, *J. Comput. Phys.*, vol. 440, pp. 110414, 2021.
- [7] Z. Geng, D. Johnson, R. Fedkiw, “Coercing Machine Learning to Output Physically Accurate Results”, *J. Comput. Phys.*, vol. 406, pp. 109099, 2020.
- [8] W. E, B. Yu, “The deep Ritz method: A deep learning-based numerical algorithm for solving variational problems”, *Commun. Math. Stat.*, vol. 6, pp. 1–12, 2018.
- [9] G. Cybenko, “Approximation by superpositions of a sigmoidal function”, *Math. Control. Signals, Syst.*, vol. 2, pp. 303–314, 1989.
- [10] K. Hornik, M. Stinchcombe, H. White, “Multilayer feedforward networks are universal approximators”, *Neural Netw.*, vol. 2, pp. 359–366, 1989.
- [11] A. Pinkus, “Approximation theory of the MLP model in neural networks”, *Acta Numer.*, vol. 8, pp. 143–195, 1999.
- [12] M. W. M. G. Dissanayake, N. Phan-Thien “Neural-network-based approximations for solving partial differential equations”, *Commun. Numer. Methods Eng.*, vol. 10, pp. 195–201, 1994.
- [13] M. Raissia, P. Perdikaris, G. E. Karniadakis, “Physics-informed neural networks: A deep learning framework for solving forward and inverse problems involving nonlinear partial differential equations”, *J. Comput. Phys.*, vol. 378, pp. 686–707, 2019.
- [14] L. Lu, P. Jin, G. Pang, Z. Zhang, G. E. Karniadakis, “Learning nonlinear operators via DeepONet based on the universal approximation theorem of operators”, *Nat. Mach. Intell.*, vol. 3, pp. 218–229, 2021.
- [15] Z. Li, N. Kovachki, K. Azizzadenesheli, B. Liu, K. Bhattacharya, A. Stuart, A. Anandkumar, “Fourier Neural Operator for Parametric Partial Differential Equations”, arXiv:2010.08895, 2020.
- [16] B. Llanas, S. Lantaron, F. J. Sainz, “Constructive approximation of discontinuous functions by neural networks”, *Neural Process Lett.*, vol. 27, pp.209–226, 2008.

- [17] R. R. Selmic, F. L. Lewis, “Neural-network approximation of piecewise continuous functions: application to friction compensation”, *IEEE Trans. Neural Netw.*, vol. 13, pp. 745–751, 2002.
- [18] M. Forti, P. Nistri, ”Global convergence of neural networks with discontinuous neuron activations”, *IEEE Trans. Circuits Syst. I*, vol. 50, pp. 1421–1435, 2003.
- [19] C. Wen, X Ma, “A max-piecewise-linear neural network for function approximation”, *Neurocomputing*, vol. 71, pp. 843–852, 2008.
- [20] Q. Liu, J. Wang, “A One-Layer Recurrent Neural Network With a Discontinuous Hard-Limiting Activation Function for Quadratic Programming”, *IEEE Trans. Neural Netw.*, vol. 19, pp. 558–570, 2008.
- [21] C. He, X. Hu, L. Mu, “A mesh-free method using piecewise deep neural network for elliptic interface problems”, *J. Comput. Phys.*, vol. 412, pp. 114358, 2022.
- [22] M.-C. Lai, C.-C. Chang, W.-S. Lin, W.-F. Hu, T.-S. Lin, A shallow Ritz method for elliptic problems with singular sources, *J. Comput. Phys.*, 469 (2022), 111547.
- [23] W.-F. Hu, T.-S. Lin, M.-C. Lai, “A discontinuity capturing shallow neural network for elliptic interface problems”, *J. Comput. Phys.*, vol. 469, pp. 111576, 2022.
- [24] B. Dong, X. Feng, Z. Li, “An FE-FD method for anisotropic elliptic interface problems”, *SIAM J. Sci. Comput.*, vol. 42, pp. B1041–B1066, 2020.
- [25] K. Lipnikov, M. Shashkov, D. Svyatskiy, Y. Vassilevski, “Monotone finite volume schemes for diffusion equations on unstructured triangular and shape-regular polygonal meshes”, *J. Comput. Phys.*, vol. 227, pp. 492–512, 2007.
- [26] F. Zhao, X. Lai, G. Yuan, Z. Sheng, “A new interpolation for auxiliary unknowns of the monotone finite volume scheme for 3D diffusion equations”, *Commun. Comput. Phys.*, vol. 27, pp. 1201–1233, 2020.
- [27] K. Pan, X. Wu, Y. Xu, G. Yuan, “An exact-interface-fitted mesh generator and linearity-preserving finite volume scheme for anisotropic elliptic interface problems”, *J. Comput. Phys.*, vol. 463, pp. 111293, 2022.
- [28] Y. Xing, H. Zheng, “A high order generalized finite difference method for solving the anisotropic elliptic interface problem in static and moving systems”, *Comput. Math. Appl.*, vol. 166, pp. 1–23, 2024.
- [29] B. Dong, X. Feng, Z. Li, “An L^∞ second order Cartesian method for 3D anisotropic interface problems”, *J. Comp. Math.*, vol. 40, pp. 882–912, 2022.

- [30] L. Li, C. Yang, “APFOS-NET: Asymptotic preserving scheme for anisotropic elliptic equations with deep neural network”, *J. Comput. Phys.*, vol. 453, pp. 110958, 2022.
- [31] D. Barreca, “A preprocessing scheme for high-cardinality categorical attributes in classification and prediction problems”, *SIGKDD Explorations*, vol. 3, pp. 27–32, 2001.
- [32] J. R. Munkres, “Topology”, Pearson College Div; 2nd edition, 2000.
- [33] M. Hou, Y. Chen, S. Cao, Y. Chen, J. Ying, ”HRW: Hybrid residual and weak form loss for solving elliptic interface problems with neural network”, *Numer. Math. Theor. Meth. Appl.*, vol 16, pp. 883-913, 2023.
- [34] C. Guo, F. Berkhahn, “Entity Embeddings of Categorical Variables”, arXiv:1604.06737, 2016.
- [35] J. J. Moré, “The Levenberg-Marquardt algorithm: implementation and theory”, *Numerical analysis*, Springer, Berlin, Heidelberg, pp. 105–116, 1978.
- [36] B. Hanin, M. Sellke, “Adam: A method for stochastic optimization”, arXiv:1710.11278, 2018.
- [37] D. Liu, J. Nocedal, “On the limited memory BFGS method for large scale optimization”, *Math. Program.*, vol 45, pp. 503–528, 1989.
- [38] B. Dong, X. Feng, and Z. Li, “An FE-FD method for anisotropic elliptic interface problems”, *SIAM J. Sci. Comput.*, vol. 42, pp. B1041–B1066, 2020.
- [39] S. Hou, W. Wang, L. Wang, “Numerical method for solving matrix coefficient elliptic equation with sharp-edged interfaces”, *J. Comput. Phys.*, vol. 229, pp. 7162–7179, 2010.